JOURNAL OF THERMOPHYSICS AND HEAT TRANSFER
Vol. 14, No. 1, January–March 2000

Coupled Dual Reciprocity Boundary Element/Finite Volume Method for Transient Conjugate Heat Transfer

Christopher P. Rahaim*
Science Applications International Corporation, Orlando, Florida 32801-2320
Alain J. Kassab†
University of Central Florida, Orlando, Florida 32816-2450
and
Robert J. Cavalleri‡
Applied Technology Associates, Inc., Orlando, Florida 32825

A coupled finite volume/dual reciprocity boundary element method is developed to solve the transient conjugate heat transfer problem of convective heat transfer over and conduction heat transfer within a solid body. In this approach, the flowfield and forced convection heat transfer external to the body is resolved by numerically solving the time-dependent Navier–Stokes equations using a finite volume method, whereas the temperature field within the body is resolved by numerically solving the heat conduction equation using a dual reciprocity boundary element method. The boundary discretization utilized to generate the computational grid for the external flowfield provides the boundary discretization required for the boundary element method. Coupling of the two fields is accomplished by enforcing interface continuity of heat flux and temperature. Transient heat transfer data needed to verify the code were obtained in a series of experiments that are reported. Details of the experimental setup and test conditions are provided. Numerical simulations of the experiments show good agreement with obtained experimental data.

Nomenclature

a = nonlinear diffusivity, function of ψ
$C(\xi)$ = free term in boundary element method (BEM) equations
c = specific heat
D = diagonal matrix
$E(x, \xi)$ = negative of normal derivative of T^* multiplied by k
e = specific energy
F = dual reciprocity BEM (DRBEM) interpolating matrix
$\boldsymbol{F}_c$ = x component of convective flux vector
$\boldsymbol{F}_d$ = x component of diffusive flux vector
f = expansion function
G = BEM influence matrix multiplying vector of nodal fluxes
$\boldsymbol{G}_c$ = y component of convective flux vector
$\boldsymbol{G}_d$ = y component of diffusive flux vector
H = BEM influence matrix multiplying vector of nodal temperatures
h = specific enthalpy
h^* = half-channel height
k = thermal conductivity
k_0 = reference thermal conductivity
L = number of additional DRBEM expansion points
N = number of BEM nodes
P = DRBEM interpolating matrix
Pe = Peclet number
Pr = Prandtl number
p = pressure
p_k = negative of normal derivative of ϕ_k multiplied by k
$\boldsymbol{q}(x)$ = heat flux vector
$r(x, \xi)$ = Euclidean distance between source (ξ) and field point (x)
T = temperature
T_B = bulk temperature
T_W = wall temperature
T_0 = reference temperature
T^* = Green's free space solution
t = time
u = x component of velocity
v = y component of velocity
$\boldsymbol{W}$ = vector of conserved variables
x = location of field point
α = dual reciprocity method expansion coefficient
Γ = boundary of domain Ω
γ = specific heat ratio
Δt = time step
θ_t, θ_q = weighting parameters in DRBEM time-marching scheme
μ = dynamic viscosity
ξ = location of source point
σ = normal viscous stress
τ = viscous shear stress
Φ = DRM interpolating matrix
ϕ = DRM expansion function
ψ = Kirchhoff parameter
ψ_0 = reference Kirchhoff parameter
Ω = domain

Presented as Paper 97-2487 at the AIAA 32nd Thermophysics Conference, Atlanta, GA, 23–25 June 1997; received 5 April 1999; revision received 19 July 1999; accepted for publication 19 July 1999.

*Senior Engineer and Chief Aerodynamicist, Missile Systems Division, 14 East Washington Street, Suite 401; christopher.p.rahaim@cpmx.saic.com.
†Associate Professor, Institute for Computational Engineering, Department of Mechanical, Materials, and Aerospace Engineering; kassab@pegasus.cc.ucf.edu.
‡President.

Introduction

NUMERICAL simulations of highly complex flow geometries are continually improving. This has been made possible by advancements in grid generation and development of robust and efficient computational algorithms. Coupled field analysis, which arises from such engineering problems as conjugate heat transfer (CHT) analysis, requires further algorithmic development. In this paper we address the solution of the transient conjugate problem: time-dependent convective heat transfer over and conduction heat transfer within a solid body. The solid body may be a cooled turbine

blade, a thrust vector control vane in a rocket, a nozzle or combustor wall; that is, the application of interest is any thermal system in which multimode heat transfer is of particular importance to thermal design. CHT arises naturally in most heat transfer applications where the external and internal temperature fields are coupled, in turbomachinery, for instance. However, conjugacy is often ignored in most numerical simulations, and a constant wall temperature or heat flux boundary condition is imposed. However, because of the maturity of current numerical methods, there has been a resurgence in interest in CHT.

There are several algorithmic approaches that can be taken to solve the conjugate problem. Most methods are based on either the finite elements method (FEM) or the finite volume method (FVM) and, in either case, require complete meshing of both fluid and solid regions while enforcing solid/fluid interface continuity of fluxes and temperatures. For instance, Comini et al.[1] develop a physically based FEM for conjugate problems requiring finite element meshing of both the solid and fluid regions. They develop separate finite element discretizations of the convective and diffusion equations and apply their technique to CHT in pipes and groundwater flow cooling of a slab. On the other hand, Shyy and Burke[2] discretize the same nondimensional energy equation for solid and liquid regions using finite volume methods and harmonic mean evaluation of interface properties. Their method requires discretization of both solid and liquid regions. They investigate effects of liquid/solid conductivity ratios on iterative convergence of relaxation schemes, and they present techniques to enhance convergence for the nonlinear conductivity case. Blank[3] adopts line successive overrelaxation to solve the implicit equations resulting from finite differencing of the convective equations on a staggered grid coupled to finite differenced equations of the radially symmetric diffusion equation by enforcement of interface continuity of temperature and heat flux. This method again requires meshing of both domains. Imlay et al.[4] and Kao and Liou[5] develop hybrid structured/unstructured grid coupling methods in an attempt to overcome difficulties arising from the tedious mesh generation required to solve heat conduction using FVM in intricate geometries such as encountered, for instance, in turbomachinery components. Imlay et al.[4] present results from a time-accurate coupled algorithm, whereas Kao and Liou[5] present steady-state results. Hassan et al.[6] develop a conjugate algorithm that is a loose coupling of an FVM-based computational fluid dynamics (CFD) code to a finite element materials response code to predict ablation profiles in hypersonic reentry vehicles. This method requires coupling of structured flow solvers and unstructured heat conduction solvers in a quasi-transient CHT solution tracing the reentry vehicle trajectory.

A different approach is taken by Li and Kassab[7] and Kassab and Li[8] which the authors develop a conjugate algorithm that does not require meshing of the solid region to resolve the heat conduction problem. In particular, the authors couple the boundary element method (BEM)[9] to an FVM Navier–Stokes solver to solve the steady-state compressible subsonic CHT problem over cooled and uncooled turbine blades. Because of the boundary-only discretization nature of the BEM, the onerous task of grid generation within intricate solid regions is avoided. Here, the boundary discretization utilized to generate the computational grid for the external flowfield provides the boundary discretization required for the BEM. In cases where the solid is multiply connected, such as a cooled turbine blade, the interior boundary surfaces must also be discretized and supplied as input; however, this poses little additional effort. Moreover, in addition to eliminating meshing the solid region, this BEM/FVM method offers an additional advantage in solving CHT problems that arises because nodal unknowns that appear in the BEM are the surface temperatures and heat fluxes. Consequently, solid/fluid interfacial heat fluxes that are required to enforce continuity in the CHT problem are naturally provided by the BEM conduction analysis, unlike FVM and FEM where heat fluxes are computed in a postprocessing stage by numerical differentiation. He et al.[10,11] adopted this approach in further studies of CHT in incompressible flow in ducts subjected to constant wall temperature and constant heat flux boundary conditions. Kontinos[12] also adopted the BEM/FVM coupling algorithm to solve the CHT over metallic thermal protection panels at the leading edge of the of the X-33 in a Mach 15 hypersonic flow regime.

In this paper we further develop the BEM/FVM coupling method to solving time-accurate CHT in compressible flows in the supersonic regime. A dual reciprocity BEM (DRBEM)[13,14] is chosen to solve transient conduction, and this code is coupled to one of two FVM Navier–Stokes solvers, GASP[15] and NASFLO.[16,17] Coupling of the two fields is accomplished by enforcing interface continuity of heat flux and temperature, and the coupling algorithm is discussed later. Each of the codes comprising the coupled DRBEM/FVM solver have been separately calibrated, and results from these codes have been reported in the literature. However, the coupled CHT solver requires validation itself, and attempts to find transient heat transfer data revealed that most available data reported in the literature are lacking all of the necessary experimental parameters, thereby rendering numerical modeling of the actual experiment impossible. Consequently, transient heat transfer data needed to verify the coupled code were obtained in a series of experiments and are reported herein. Three wind-tunnel models were used to obtain transient data for validation: a 10-deg sharp cone and a three-dimensional 12.5-deg blunted cone cylindrical model were instrumented and used for wind-tunnel calibration, whereas a two-dimensional 12.5-deg blunted wedge was used for the conjugate experiment. The sharp nose cone was instrumented with pressure taps, whereas the blunt nose test models were instrumented with thermocouples and pressure taps. The University of Central Florida (UCF) high-speed wind tunnel was used to gather experimental data. Test runs were performed at a supersonic Mach number to trace transient temperatures within and pressures over the test models. Numerical simulations of the experiments were also undertaken, and details of the experimental setup, test conditions, and relevant parameters are provided. Experimental data and numerical CHT modeling predictions were shown to be in close agreement, thus, verifying the accuracy of the proposed DRBEM/FVM conjugate solver.

Governing Equations and Numerical Algorithm

The governing equations for the fluid flow are the compressible time-dependent Navier–Stokes equations, whereas the transient heat conduction equation is used to resolve the temperature field in the solid region. These two codes are coupled by enforcing fluid/solid interface continuity of temperature and heat flux. Each code is described separately and the coupling algorithm is then provided.

Fluid Flow and Navier–Stokes Solvers

Problems considered in this paper are two dimensional, although the proposed approach is not limited to two dimensions. The governing equations for external fluid flow and heat transfer are the time-dependent compressible Navier–Stokes equations that can be written in integral form as

$$\int_{\Omega} \frac{\partial \boldsymbol{W}}{\partial t}\,\mathrm{d}V + \int_{\Gamma} (\boldsymbol{F}\,\mathrm{d}y - \boldsymbol{G}\,\mathrm{d}x) = 0 \tag{1}$$

where Ω in this case is the finite volume domain and Γ is the bounding surface of the domain (finite volume) Ω. In a two-dimensions, the vectors $\boldsymbol{F}$ and $\boldsymbol{G}$ are

$$\boldsymbol{F} = \boldsymbol{F}_c + \boldsymbol{F}_d, \qquad \boldsymbol{G} = \boldsymbol{G}_c + \boldsymbol{G}_d \tag{2}$$

$$\boldsymbol{W} = \begin{bmatrix} \rho \\ \rho u \\ \rho v \\ \rho e \end{bmatrix}, \qquad \boldsymbol{F}_c = \begin{bmatrix} \rho u \\ \rho u^2 + p \\ \rho uv \\ \rho uh \end{bmatrix}, \qquad \boldsymbol{G}_c = \begin{bmatrix} \rho v \\ \rho uv \\ \rho v^2 + p \\ \rho vh \end{bmatrix} \tag{3}$$

$$\boldsymbol{F}_d = \begin{bmatrix} 0 \\ \sigma_{xx} \\ \tau_{xy} \\ u\sigma_{xx} + v\tau_{xy} - k\dfrac{\partial T}{\partial x} \end{bmatrix}, \qquad \boldsymbol{G}_d = \begin{bmatrix} 0 \\ \tau_{xy} \\ \sigma_{yy} \\ v\sigma_{yy} + u\tau_{xy} - k\dfrac{\partial T}{\partial y} \end{bmatrix} \tag{4}$$

where ρ is the density and μ is the dynamic viscosity of the fluid. We employ the Baldwin–Lomax[18] algebraic turbulence model to calculate eddy viscosity and turbulent transport coefficients. The effective viscosity and thermal conductivity are given by

$$\mu = \mu_l + \mu_t, \qquad k = \gamma/(\gamma - 1)[(\mu_l/Pr_l) + (\mu_t/Pr_t)] \tag{5}$$

where the subscripts l and t are laminar and turbulent values, respectively. The turbulent Prandlt number is set to 0.9 (Ref. 19), and the laminar Prandtl number was set to 0.71 for air.

In both the NASFLO and GASP solvers used in this study, the Navier–Stokes equations were discretized using a cell-centered FVM. NASFLO[16,17] uses an implicit upwind scheme based on the flux vector splitting method described by Whitfield[20] and Whitfield and Janus[21] along with a min-mod flux limiter. GASP is also an implicit code using approximate factorization, and it was run in all cases reported herein under the Van Leer flux-vector splitting option with a min-mod flux limiter. Both codes use the Baldwin–Lomax[18] turbulence model.

Heat Conduction and DRBEM Solver

The governing equation for temperature in an isotropic heat conducting medium with no energy generation is

$$\nabla \cdot (k\nabla T) = \rho c \frac{\partial T}{\partial t} \tag{6}$$

In the BEM, transient problems can be solved by one of three basic methods. In the first, a transient fundamental solution is used to generate a corresponding transient boundary integral equation.[9] The second approach uses the Laplace transform to convert the transient problem to a boundary value problem in Laplace space, which is solved by BEM, and the solution is subsequently inverted back to real time numerically.[22] The third approach relies on the steady-state fundamental solution of the corresponding steady-state equation and the dual reciprocity method to expand the time derivative.[14] Here, we adopt the latter method and briefly review the DRBEM formulation for heat conduction in which the right-hand side of the diffusion equation (6) is first expanded in series as

$$\rho c \frac{\partial T}{\partial t} = \sum_{k=1}^{N+L} \alpha_k \nabla^2 \phi_k \tag{7}$$

where N is the number of BEM boundary nodes at which dual reciprocity points are collocated and L is the number of additional internal dual reciprocity points. The functions u_k are defined shortly. Substitution of Eq. (7) into Eq. (6) leads to

$$k\nabla^2 T = \sum_{k=1}^{N+L} \alpha_k \nabla^2 \phi_k \tag{8}$$

We consider a two-dimensional problem. Consequently, we multiply both sides of Eq. (8) by the two-dimensional fundamental solution to the Laplace equation, $T^*(x, \xi) = -\ell n\, r(x, \xi)/2\pi k$, where r is the radial distance between the field point x and the source point ξ, and by integrating over the domain, there results

$$\int_\Omega T^*(x, \xi)[k\nabla^2 T(x)]\, \mathrm{d}\Omega = \sum_{k=1}^{N+L} \alpha_k \int_\Omega T^*(x, \xi)\nabla^2 \phi_k(x)\, \mathrm{d}\Omega \tag{9}$$

By application of Green's first identity twice to both sides of Eq. (9),

$$C(\xi)T(\xi) + \oint_\Gamma [q(x)T^*(x, \xi) - E(x, \xi)T(x)]\, \mathrm{d}\Gamma = \sum_{k=1}^{N+L} \alpha_k \left\{ C(\xi)\phi_k(\xi) + \oint_\Gamma \frac{1}{k}\left[p_k(x)T^*(x, \xi) - E(x, \xi)\phi_k(x)\right] \mathrm{d}\Gamma \right\} \tag{10}$$

where the following notation is used: $q(x) = -k\nabla T \cdot \hat{n}$, $p_k(x) = -k\nabla \phi_k \cdot \hat{n}$, and $E(x, \xi) = -k\nabla T^* \cdot \hat{n}$. The outward-drawn normal to the boundary Γ is $\hat{n}$. The free term $C(\xi)$ is equal to one when the source point ξ lies within the domain, and it is equal to the angle by which the local tangent turns at the source point ξ divided by 2π when ξ lies on the boundary. After introducing a pattern of N boundary nodes and introducing boundary elements to model the boundary geometry and temperature and flux distributions, Eq. (10) can be expressed in matrix form as shown by Partridge et al.[14]:

$$G\boldsymbol{q} - H\boldsymbol{T} = \sum_{k=1}^{N+L} \alpha_k \{G\boldsymbol{p}_k - H\boldsymbol{\phi}_k\} \tag{11}$$

The influence coefficient matrices G and H are evaluated numerically using adaptive Gauss-type quadratures. In this work, subparameteric constant elements are used consistently. The geometry is modeled using linear shape functions, whereas the temperature and flux are modeled as piecewise constant over each boundary element. The use of subparametric elements in the BEM discretization is advantageous for the application at hand. In particular, such elements have the unknown located at the center of the element and match the cell-centered geometric arrangement of the FVM code, thus offering a seamless means of matching both codes. From Eq. (7), the vector α_k can be expressed as

$$\rho c \frac{\partial T}{\partial t} = \sum_{k=1}^{N+L} \alpha_k f_k \tag{12}$$

where the functions f_k satisfy the following: $f_k = \nabla^2 \phi_k$. Collocating Eq. (12) at the $N + L$ dual reciprocity expansion points leads to

$$\rho c \left(\frac{\partial T}{\partial t}\right) = F\alpha \tag{13}$$

Inverting the interpolating matrix F to solve explicitly for the vector of expansion coefficients α allows Eq. (11) to be recast as

$$H\boldsymbol{T} - G\boldsymbol{q} = C\left(\frac{\partial T}{\partial t}\right) \tag{14}$$

where the capacitance matrix C is

$$C = -\rho c\{GP - H\Phi\}F^{-1} \tag{15}$$

where the matrices Φ and P are obtained by evaluating the expansion functions ϕ_k and their normal derivatives p_k at every dual reciprocity point, respectively. The final step in DRBEM for the diffusion equation involves the finite differencing of the temporal derivative in Eq. (14) and the approximation of the nodal temperatures and fluxes. Applying a first-order finite difference in time and using parameters θ_t and θ_q to position the temperature vector $\boldsymbol{T}$ and the flux vector $\boldsymbol{q}$ between the time steps p and $p + 1$ yields

$$(\Delta t\theta_t H - C)\boldsymbol{T}^{p+1} - (\Delta t\theta_q G)\boldsymbol{q}^{p+1} = [\Delta t(\theta_t - 1)H - C]\boldsymbol{T}^p + \Delta t(1 - \theta_q)G\boldsymbol{q}^p \tag{16}$$

where the right-hand side is known from the previous time step p. On introduction of the boundary conditions, Eq. (16) is solved for the temperature evolution. In our code we use a fully implicit formulation, θ_t and $\theta_q = 1$. Note that the DRBEM equations provide the time history of boundary temperature and heat fluxes in the solution process [Eq. (16)]. The dual reciprocity expansion functions f_k that are used are the standard radial basis functions,[23] $f_k = r_k + 1$, where r_k is the radial distance from every field point to the kth dual reciprocity point. The expressions p_k and ϕ_k follow from their definitions.

Another advantage of using the DRBEM for transient conduction is that the nonlinear heat conduction problem can be accommodated for those cases encountered in a high-temperature environment for which the variation of k with temperature is significant. In such cases, the classical Kirchhoff transformation[24] is first applied to define a new dependent variable ψ through the relation, $\mathrm{d}\psi/\mathrm{d}T = k(T)$. Thus, this transformation defines ψ as a single-valued monotonically increasing function of T that is actually the integral of the k vs T curve:

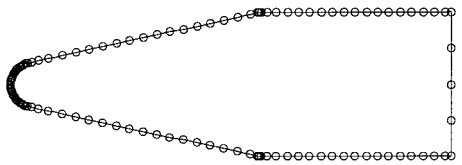

a) DRBEM grid for numerical solution of heat conduction equation

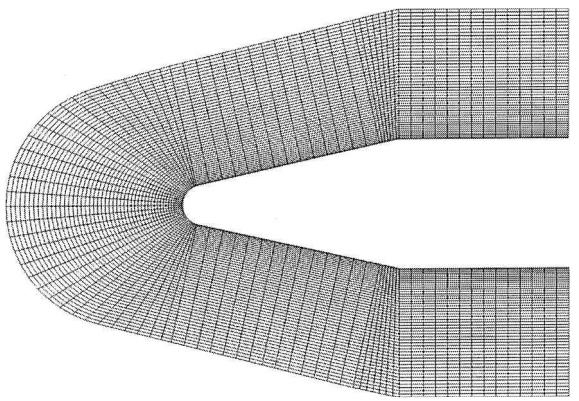

b) Finite volume flow solver grid

Fig. 1 Grids used in conjugate study of blunted wedge.

$$\psi(T) = \frac{1}{k_0}\int_{T_0}^{T} k(T)\,\mathrm{d}T + \psi_0 \tag{17}$$

where $k_0 = k(T_0)$ and ψ_0 is an arbitrary reference value. This classical transformation reduces the diffusion equation to

$$\nabla\cdot(k_0\nabla\psi) = \frac{k_0}{a(\psi)}\frac{\partial\psi}{\partial t} \tag{18}$$

where $a(\psi) = k(\psi)/\rho(\psi)c(\psi)$. In steady state, the transformation linearizes the governing equation; however, in the transient case, the nonlinearity is not completely eliminated. By the using of the reference thermal conductivity in evaluating the fundamental solution $T^*(x, \xi)$, a dual reciprocity equation of the form of Eq. (16) is obtained for the new dependent variable ψ and its normal derivative. However, as the left-hand side of Eq. (12) is replaced by $k_0/a(\psi)\partial\psi/\partial t$, the capacitance matrix C implicitly depends on the variable ψ, and it is redefined as

$$C = -\{GP - H\Phi\}F^{-1}D \tag{19}$$

where D is a diagonal matrix whose elements are $k_0/a(\psi)$ evaluated at each collocation point. Thus, the time-accurate diffusion solution in this case requires a sublevel iteration at each time level in which the capacitance matrix is updated. Brebbia and Nowak[25] discuss the details of a Newton–Raphson method for this step. The DRBEM code used in this work has been thoroughly tested, and results of heat conduction analysis are reported by Rahaim[26]; extensions of the DRBEM code to the solution of incompressible flows in unheated and heated channels are also reported by Rahaim and Kassab.[27–29] A typical BEM surface grid used to solve heat conduction for the CHT problem over a two-dimensional blunted wedge considered in this study is shown in Fig. 1a along with the corresponding FVM mesh used for the NS solution that is displayed in Fig. 1b.

DRBEM/FVM Conjugate Code

Two conjugate FVM/BEM codes were developed from this study, and they are identified as DRBEM/GASP and DRBEM/NASFLO, inasmuch as the first couples GASP with the DRBEM code described earlier, and the second couples NASFLO with the DRBEM code. Coupling of the two fields is accomplished by enforcing interface continuity of heat flux and temperature at each time step. The general procedure followed for the coupling of the flow solver and heat conduction solver is outlined as follows:

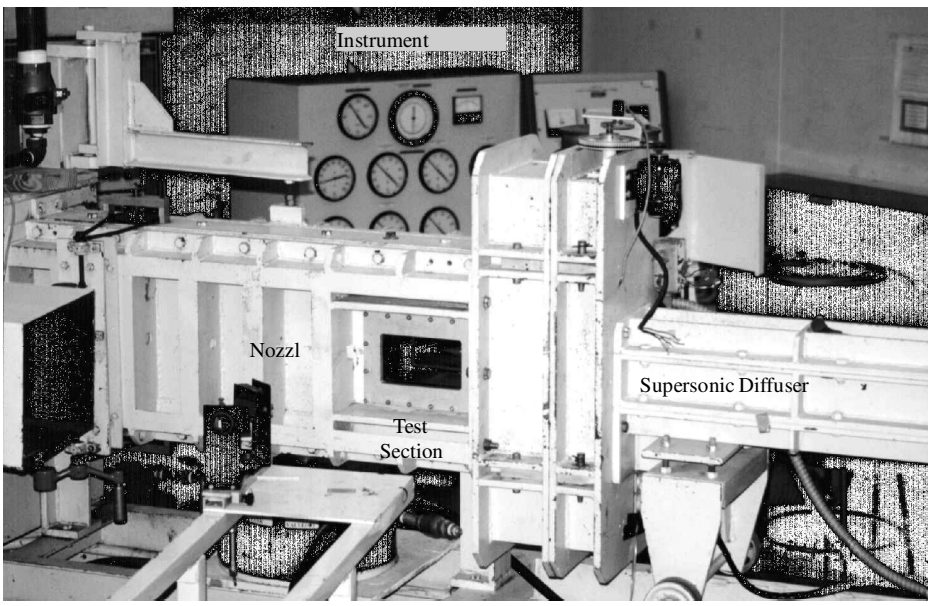

Fig. 2 Supersonic wind tunnel.

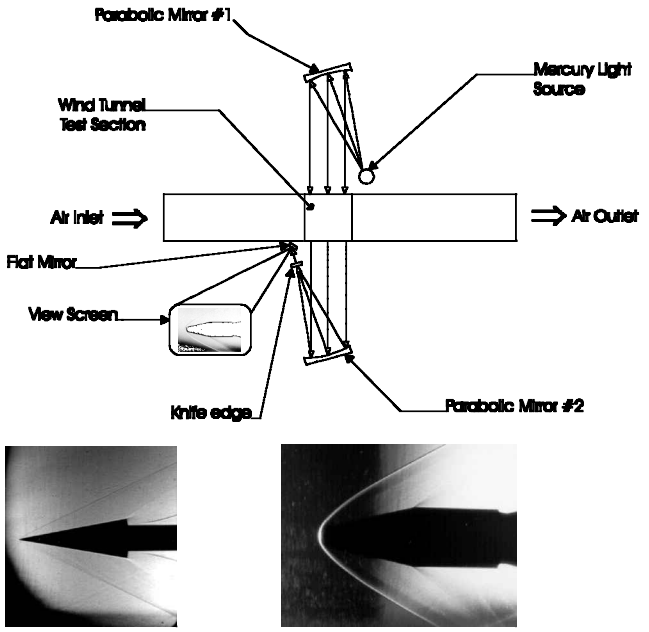

Fig. 3 Schlieren visualization system configuration with schlieren photograph of the calibration sharp nose cone (left) and the blunted wedge (right) under settings used in the experiments.

1) By use of the CFD code, for a given solid region surface temperature distribution, solve for the current flowfield conditions.

2) Send the heat transfer code the newly calculated values of flowfield variables.

3) Calculate the surface heat flux value for the solid region and set this as the boundary condition for solution of the temperature field of the solid body.

4) Use the DRBEM to calculate the new temperature field for the solid body including a new surface temperature distribution.

5) Send the CFD code the new surface temperature distribution.

6) Repeat steps 1–5 for each time step.

Note that the CFD code is the limiting factor in time-accurate computations. For instance, a time-accurate solution required a time step of $\Delta t = 10^{-5}$ s in the simulations to be reported. Once the matrix equations are assembled, each BEM run requires the solution of a linear algebraic set whose dimension is the number of nodes used to discretize the surface. In the cases to be reported, the linear set is 50×50, which is readily solved by a direct lower/upper (LU) decomposition. Furthermore, as the LU factors are available after the first step, subsequent conduction solutions are obtained by simple forward and backward substitution at each time step. Thus, the computational burden of the CHT algorithm described earlier is predominantly due to the CFD solution, whereas the DRBEM conduction solution places a miminal burden on the process. This completes the description of the CHT solver. Attention is now given to experiments carried out to generate heat transfer data that are to be used for conjugate code validation.

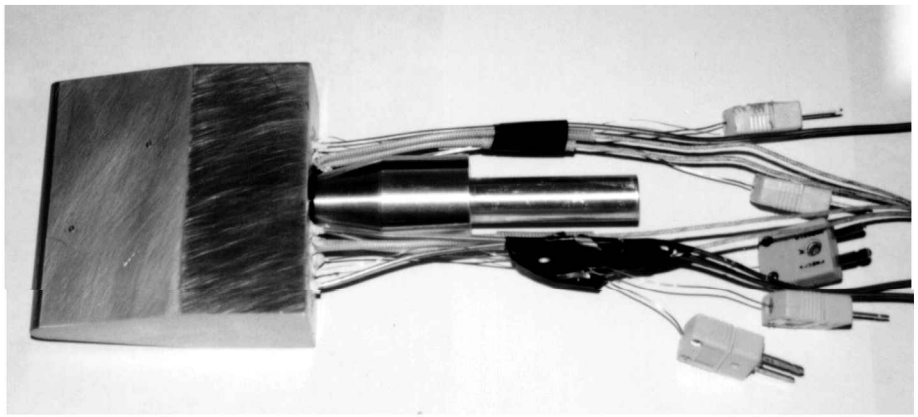

a) Fully instrumented model

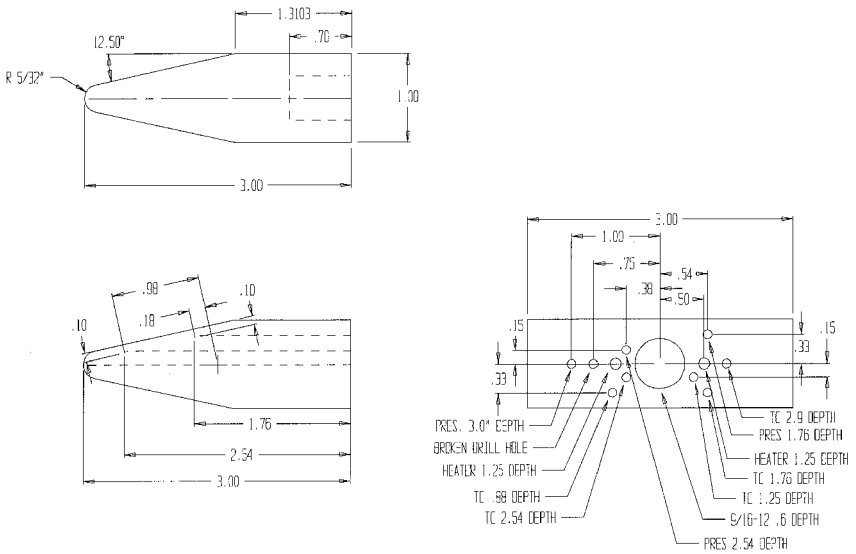

b) Dimensions (in.) and tap locations

Fig. 4 Blunted wedge model.

Experimental System

The three wind-tunnel models used to obtain transient data using the high-speed wind-tunnel facility at UCF are a 10-deg sharp cone, a two-dimensional 12.5-deg blunted wedge, and a three-dimensional 12.5-deg blunted cone cylindrical configuration. The sharp nose cone was instrumented with pressure taps, whereas the blunt nose test models were instrumented with thermocouples and pressure taps. Test runs were performed at several Mach numbers to trace transient temperature within and pressures over the test models. In the following sections, the facilities used, construction of the wind-tunnel models, model instrumentation, and experimental procedure are discussed.

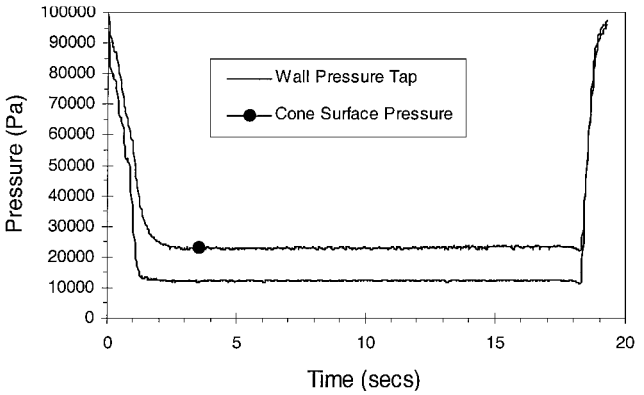

Fig. 5 Pressure readings from data acquisition system during the sharp cone model wind-tunnel test.

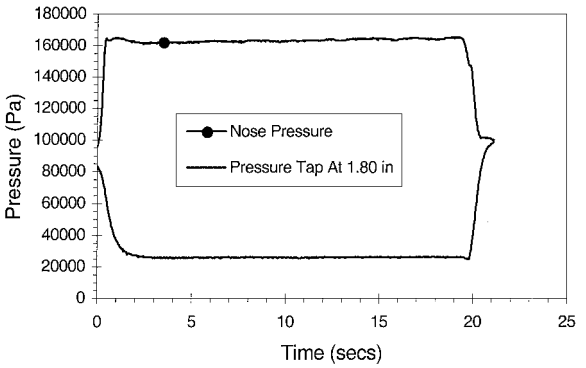

Fig. 6 Pressure readings from data acquisition system during the blunted cone model wind-tunnel test.

Facilities

The UCF supersonic testing facilities include a high-speed wind tunnel, a visualization system, and a data acquisition system. The high-speed wind tunnel is a 4-in. supersonic conventional blowdown single-pass design capable of generating Mach numbers in the range of 1.5–5.0. The blowdown air is supplied from a compressor/storage tank combination. A 150-hp two-stage compressor regulated at a maximum pressure of 220 psi supplies air to a 329-ft^3 storage tank. An automatic feedback system between the stilling chamber and the main 4-in. double-ported control valve is used to regulate the stagnation pressure supplied to the tunnel. A flexible nozzle is used to vary the entrance area of the test section. A view of the supersonic wind tunnel is provided in Fig. 2.

A continuous slit source schlieren optical system was used to visualize the flow in the test section. The system consists of a 1000-W BH6 mercury vapor light source, two 6-in., 48-in. focal length parabolic mirrors, a flat mirror, a knife edge, and a viewing screen. A diagram showing the schlieren system setup is in Fig. 3, along with a schlieren photograph showing a bow shock on the two-dimensional blunted wedge model during a Mach 3 run. A number of photographs and a videotape were taken during the course of experiments for later comparison with CFD results.

A personal computer-based data acquisition system was used to acquire data from the model instrumentation and to keep track of the tunnel stagnation temperature. This system consists of a 100-MHz Pentium personal computer with a 1.2-GB HD and an A/D board with an expansion chassis. The ADAC Corporation 5525MF A/D high-speed board with high-level 16-channel multiplexed A/D converter with programmable gain was interfaced with the personal computer via an open industry standard architecture bus slot. The expansion chassis connects to the 5525MF A/D board via a 50-pin ribbon cable. This expansion chassis provides an additional 16 fully differential analog inputs capable of holding a number of different signal conditioning modules. The module used in the expansion chassis was an ADAC Corporation 4012TCEX. This module provides for low-level input, as well as thermocouple input with cold junction. LabTech Notebook version 8.01 for windows was used to operate the A/D board and to gather data.

Wind-Tunnel Models

Three wind-tunnel models were used. These models included a sharp cone, a blunted wedge, and a blunted cone cylinder. The

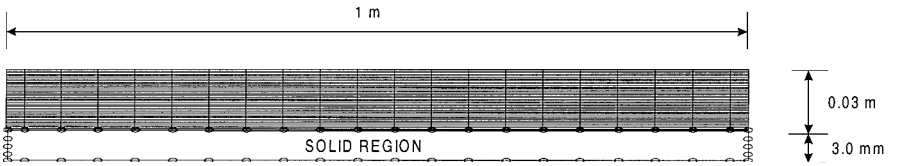

a) DRBEM and FVM grids used in CHT problem over a flat plate

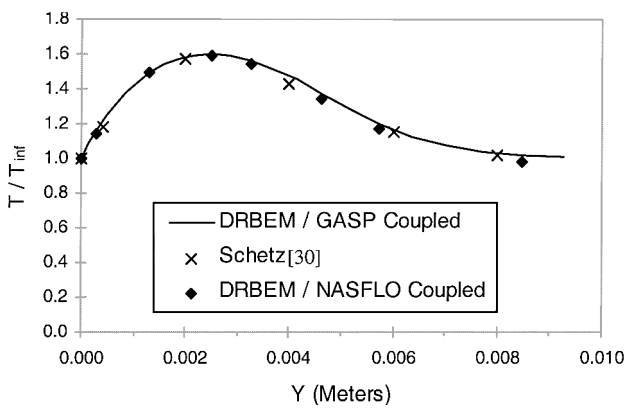

b) Comparisons of conjugate code predicted temperatures with experimental results

Fig. 7 Comparison of temperature profile at $x = 1$ m under $M = 4.0$ flow conditions.

sharp cone was supplied with the wind tunnel as a standard test model to characterize the flowfield. The blunted wedge was constructed of 6064-T6 aluminum, for which the material properties are $k = 167$ W/mK, $\rho = 2790$ kg/m^3, and $c = 883$ J/kgK. A photograph of the instrumented blunted wedge model is shown in Fig. 4a, and the blunted wedge dimensions are provided in Fig. 4b. The third model was a blunted-conecylinder configuration instrumented with heating elements. The blunted cone cylinder model was constructed of 2024 aluminum, for which the material properties are $k = 177$ W/mK, $\rho = 2770$ kg/m^3, and $c = 875$ J/kgK. Dimensions, tap and thermocouple locations, and a photograph of the cone can be found in Ref. 26.

Instrumentation

All three models were instrumented to measure pressures and/or temperatures. The sharp cone model was only instrumented with surface pressure taps. A series of pitot tubes, connected to the surface pressure taps, lead out of the model through the sting. Surface pressures were read using Motorola MPX700 series uncompensated silicon pressure sensors. This pressure sensor is capable of measuring from 0 to 100 psi. The millivolt signal output by the sensor is a linear voltage output that is directly proportional to the applied pressure. The output voltage of the sensor was connected to the 4012TCEX module for continuous data sampling during the wind-tunnel run. The blunted wedge and blunted cone models used were instrumented with both surface pressure taps and type-K thermocouples of 0.020-in. diameter. Locations of the surface pressure taps and thermocouples for the blunted wedge are shown in Fig. 4. The pitot tubes, thermocouples, and heaters were attached to the aluminum models using a high-temperature, thermal conductive epoxy. The thermocouples were mounted in the interior of the model so that temperatures recorded in the experiments could be compared with temperatures predicted by the DRBEM/FVM conjugate code. The thermocouples were connected to the 4012TCEX module and sampled against the cold junction for continuous temperature readings during the wind-tunnel run. The surface pressure was measured in the same manner as was outlined for the cone.

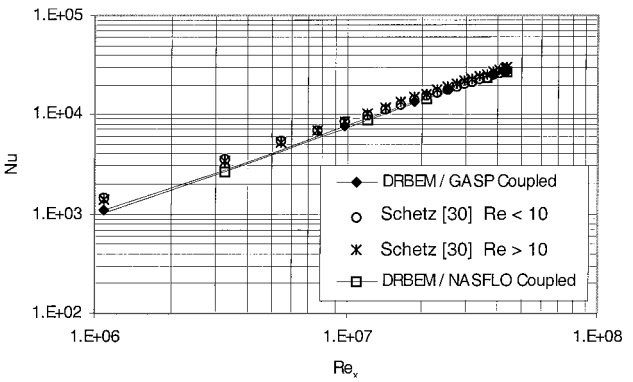

Fig. 8 Comparison of Nusselt number for turbulent supersonic flow over a flat plate with $M = 2.0$.

Experimental Procedure

Because the purpose of the experimental effort was to gather experimental data to be used to validate the computational results, it is imperative to know the flow conditions. The necessary parameters for numerical modeling of the experiment can be obtained by characterizing the flowfield. Parameters required in numerical modeling are the stagnation pressure, stagnation temperature, and Mach number. The stagnation pressure was read from the pressure gauge located on the instrumentation console of the wind tunnel. The stagnation temperature was measured during the wind-tunnel run using a type-K thermocouple mounted in the settling chamber.

The last parameter needed for accurate numerical modeling is the test section Mach number. Three methods were used to determine the Mach number: 1) measurement of the freestream or wall static pressure and comparison to the tunnel stagnation pressure using the Rayleigh pitot formula, 2) measurement of shock wave angle of a sharp cone and comparison of the angle to cone theory, and 3) measurement of the stagnation pressure downstream of the shock formed ahead of the model and comparison with the tunnel stagnation pressure. The 10-deg cone model was used first. After setting up the instrumentation and calibrating the pressure readings, one channel was connected to the surface tap located 1.280 in. from the front of the model to read surface pressure. A second channel was connected to a static tap located on the lower wind-tunnel wall aligned with the front of the test section. The pressure data are given in Fig. 5. Taking the static pressure tap data and comparing to the total pressure of the stilling chamber gives a Mach number of 3.03. Shock wave angle off the cone is measured as 22 deg from a schlieren photograph (see lower left of Fig. 3), which gives a Mach number of 3.1. Next, calculating the cone surface pressure based on this Mach number leads to a static pressure value of 18,995 Pa. Examination of Fig. 5 indicates that this value is within 16% of the measured value. Comparison of the measured wall static pressure (11,997 Pa) with the wind-tunnel console gauges (12,273 Pa) determined that the data acquisition system and console gauge had a margin of error less than 2%.

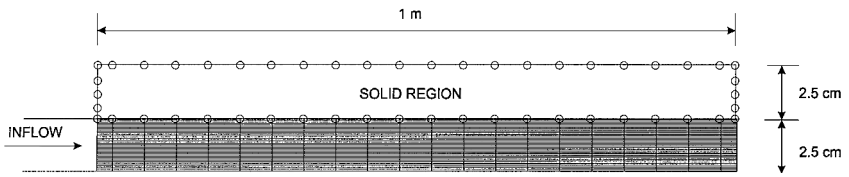

a) Geometry and grids used to model CHT in laminar duct flow problem

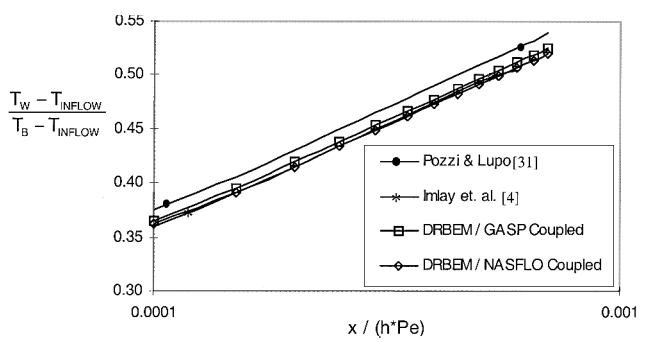

b) Comparison of nondimensional wall temperature predictions

Fig. 9 Comparison of DRBEM/GASP and DRBEM/NASFLO nondimensional wall temperature predictions for conjugate heat transfer in laminar duct flow with $M = 0.2$.

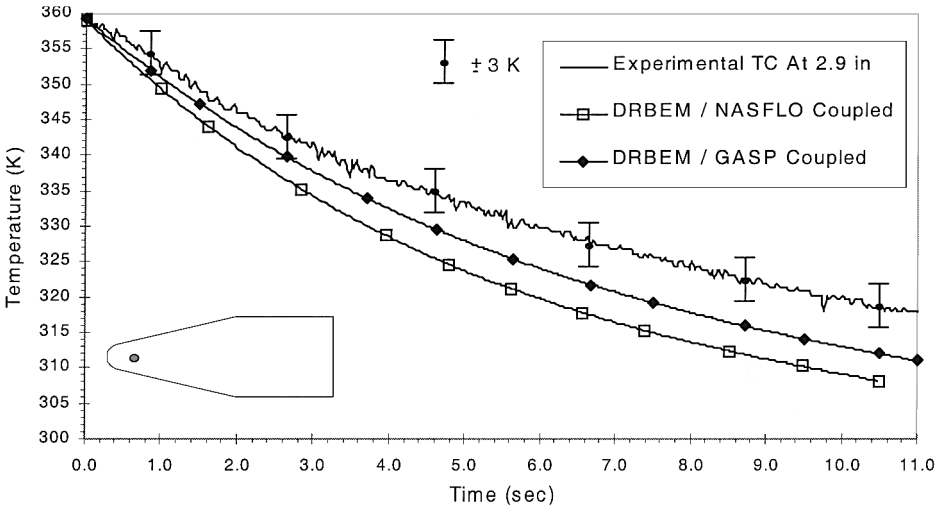

a) Thermocouple located at 2.9 in.

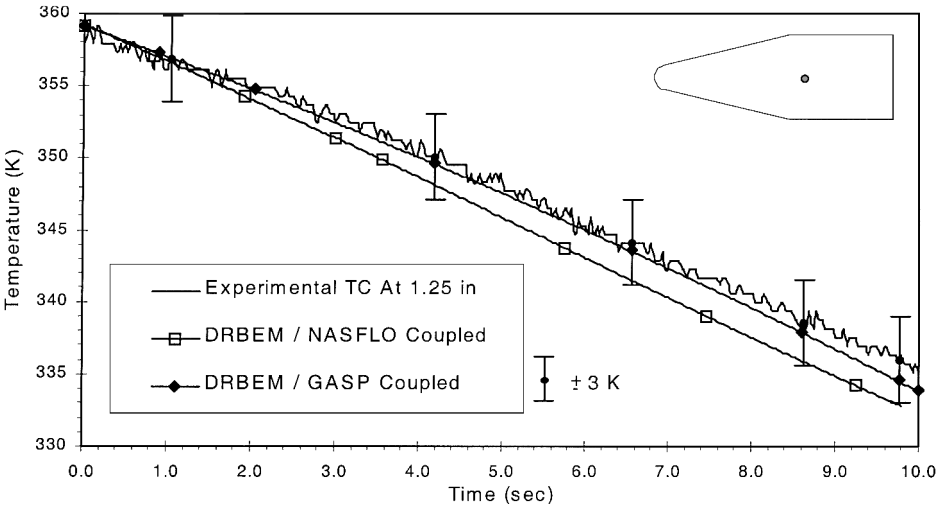

b) Thermocouple located at 1.25 in.

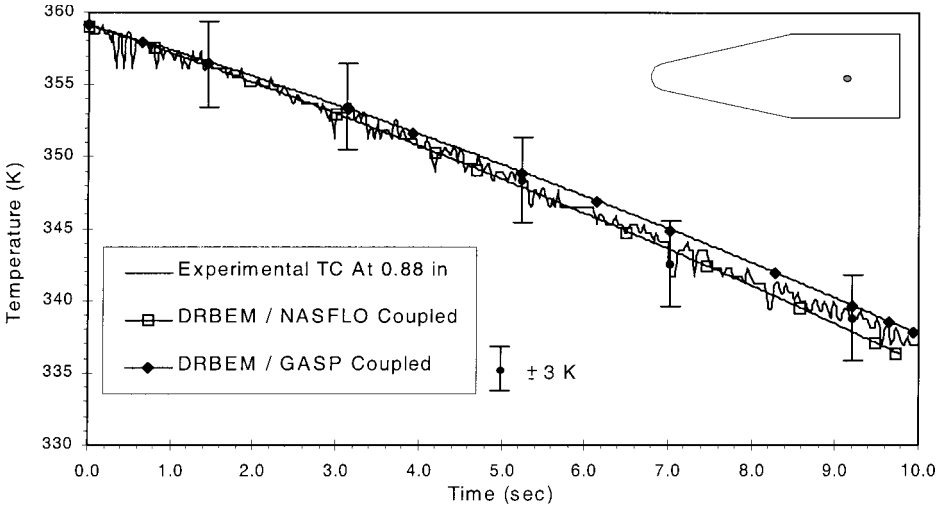

c) Thermocouple located at 0.88 in.

Fig. 10 Comparison of conjugate transient temperature predictions with experimental results for the blunted wedge model at $M = 3.03$ flow conditions.

By using the Mach number value of 3.03 and by knowing the total pressure and temperature, the wind-tunnel flow characteristics can be summarized as given in Table 1. By the use of these conditions as input, a computational run using GASP was made for the sharp cone model. In this run, a Baldwin–Lomax turbulence model was used with Van Leer flux-vector split and min-mod limiter. The results showed a surface pressure of 18,891 Pa. This result serves to confirm measured wind-tunnel values.

Finally, the axially symmetric blunt cone cylinder model was used as an additional verification of flowfield conditions. The blunt nose is instrumented with a pressure tap. An accurate measure of the Mach number can be obtained by comparing the total pressure behind the shock with the total pressure forward of the shock. One channel of the instrumentation was connected to the total pressure tap, and a second channel was connected to the surface pressure tap located 1.80 in. from the back surface of the blunt cone cylinder. A trace showing the measured pressures is given in Fig. 6. Comparing the stagnation pressure of the nose with the stilling chamber gives a Mach number of 2.96. Good agreement between all three methods establishes the validity of the flow conditions listed in Table 1. Results of verification studies of the DRBEM/FVM conjugate algorithm are now presented.

Table 1 Wind tunnel conditions used for numerical modeling $M = 3.03$

Total/stagnation	Static
$T_0 = 293.15$ K	$T = 103.32$ K
$P_0 = 468{,}860$ Pa	$P = 12{,}185$ Pa
$\rho_0 = 5.5727$ kg/m^3	$\rho = 0.4109$ kg/m^3

Coupled DRBEM/FVM Transient Conjugate Code Verification

The first verification of the DRBEM/FVM codes was made for steady-state conditions for which data are available for comparison. Here, the conjugate code is marched in time until the variables converge to steady conditions. The first case considered is flow over a very thin aluminum flat plate with an imposed isothermal boundary condition at the lower surface. The geometry and FVM and DRBEM grids are shown in Fig. 7a. For this case, the flow Mach number was 4.0, with freestream pressure of 0.01 atm and a static temperature of 300 K. These conditions give a Reynolds number of 88,535 based on the length of the flat plate, ensuring a laminar flow regime over the length of the plate. The temperature applied to the underside of the plate was 300 K. The results for this case are shown in Fig. 7b, with very good agreement with results reported by Schetz[30] for flow over an isothermal flat plate. Next, to validate CHT modeling capabilities of the DRBEM/FVM codes in turbulent flow, both versions were used with the Baldwin–Lomax[18] model to predict the Nusselt number for turbulent flow over a flat plate. The geometry and grids were the same as those shown in Fig. 7a. The flow conditions were a Mach number of 2.0, a freestream density of

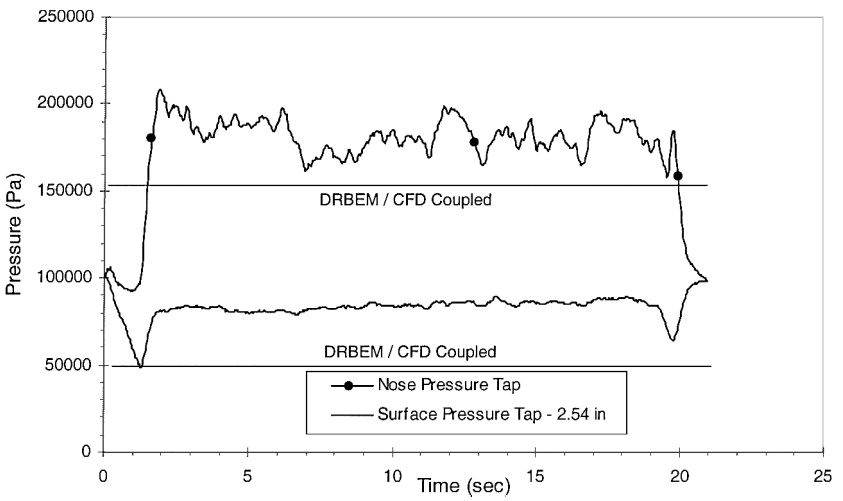

Fig. 11 Pressure trace from experimental data over length of wind-tunnel run compared with solution of coupled code for $M = 3.03$.

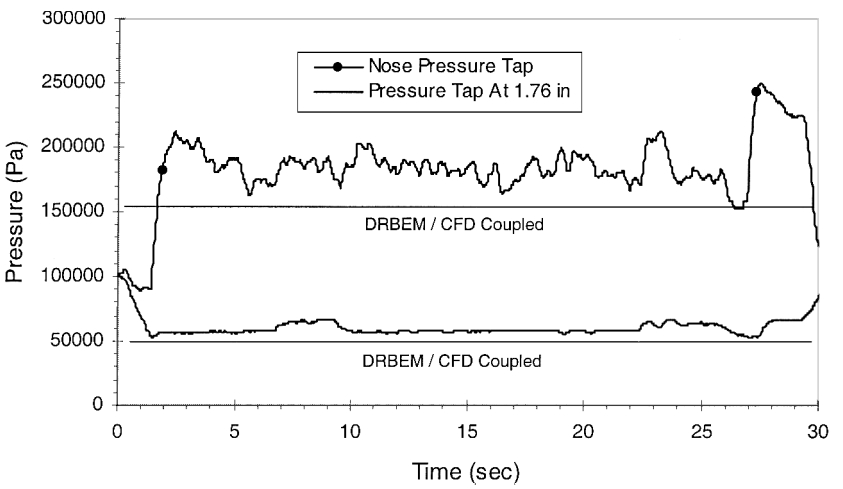

Fig. 12 Pressure trace from experimental data for tap at 1.76 in. over length of wind-tunnel run compared with solution of coupled code for $M = 3.03$.

1.16 kg/m^3, and a stagnation temperature of 540 K. In this case, the back side of the flat plate was also maintained at constant temperature of 300 K. Conjugate code-computed Nusselt distributions over the flat plate are compared in Fig. 8 with those reported by Schetz.[30] Here again, both codes provide good predictions. Finally, a CHT problem in a laminar duct is considered. The geometry used for this case is shown in Fig. 9a, with only one-half of the duct displayed. The inflow conditions used in this example were $M = 0.2$ with a temperature of 300 K. The back side of the solid region, T_B, was maintained at 320 K. The thermal conductivity of the flowing gas was that of air at 300 K, which is 0.02617 W/mK, and the thermal conductivity of the solid region was taken as 0.2617 W/mK. Results for this case are shown in Fig. 9b compared with the analytical solution of Pozzi and Lupo[31] and a computational solution of Imlay et al.[4] Here the position down the duct is given as a nondimensional value, where x is the dimensional horizontal position. The results of the present code are in excellent agreement with published results for the solid/fluid interface temperature T_w. Now that the conjugate code results for steady-state analysis are verified, attention is given to transient problem verification.

We now report on results from numerical simulations of the high-speed wind-tunnel tests for the blunted wedge model that were performed using the flow conditions given in Table 1. The blunted wedge was heated uniformly to a temperature of 359 K, as indicated by all three thermocouples. Subsequently the wind tunnel was started to establish the flow conditions reported in Table 1, and the

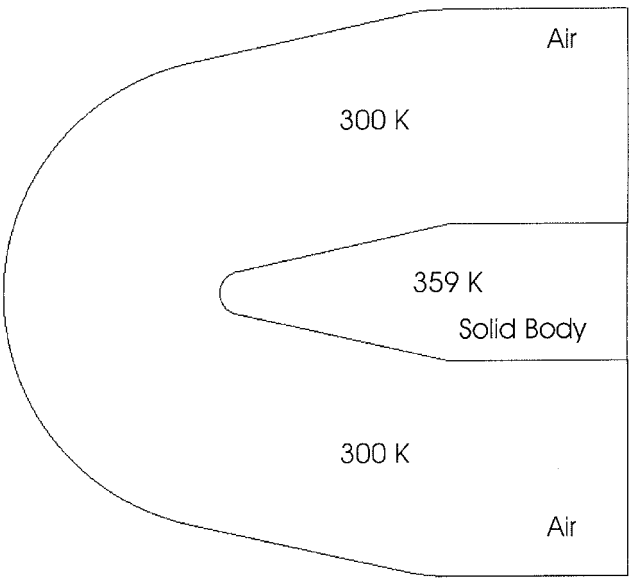

a) Partial flowfield domain and solid body outline showing initial temperatures for $t = 0$ s

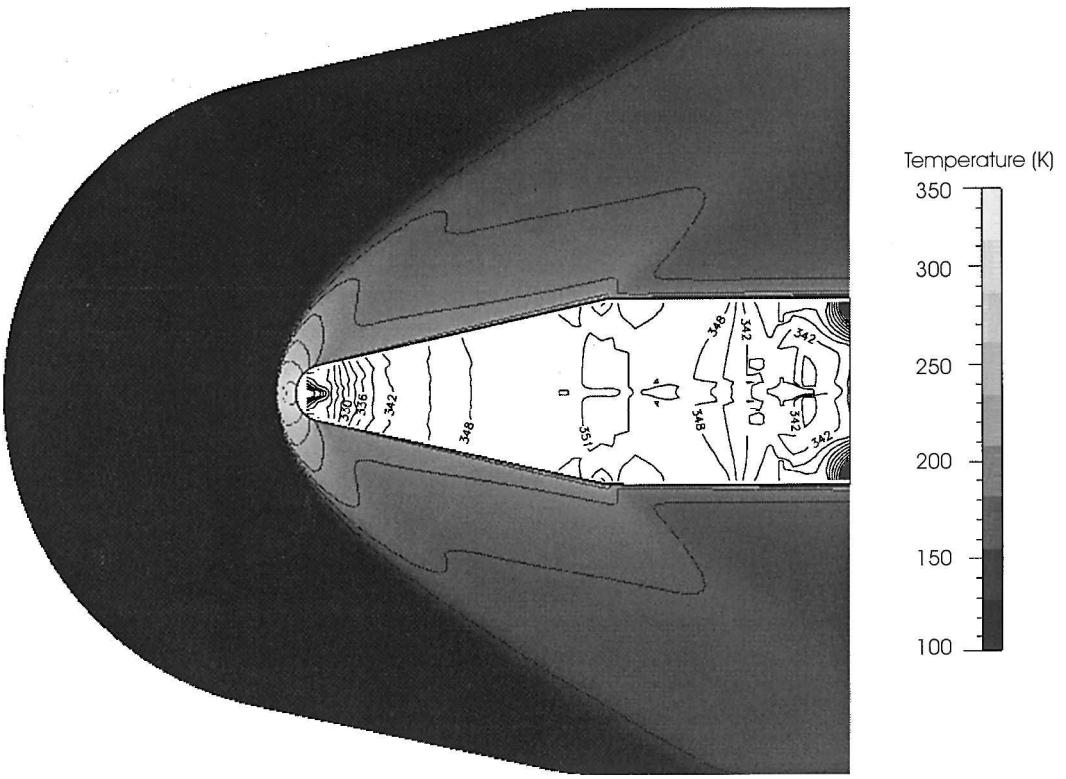

b) Partial flowfield domain and solid body contours of temperature for $t = 5.4$ s

Fig. 13 Conjugate study showing temperature at $t = 0$ and 5.4. s.

blunted wedge was allowed to cool. Temperature traces obtained from the three thermocouples installed in the wedge along with corresponding temperature predictions from both versions of the coupled DRBEM/FVM conjugate code are provided in Figs. 10a–10c. Examination of Figs. 10 reveals that both conjugate codes are capturing the trend and magnitude of the data, with the GASP version giving closer results to experimental values. Figure 11 shows a pressure trace for the stagnation pressure tap and the surface pressure tap located 2.54 in. from the backsurface of the model. Figure 12 shows a pressure trace for the stagnation pressure tap and the surface pressure tap located at 1.76 in. from the back surface of the model. Both coupled code versions predict a stagnation pressure of 160,000 Pa; however, experimental measurement is nearly 30,000 Pa higher than the coupled code prediction. Further, the two runs reported in Figs. 11 and 12 reveal consistent results for the stagnation pressures. An explanation for the higher experimental value of the stagnation pressure is provided by consideration of the width of the wedge relative to the test section. In particular, end effects were significant because the wedge model was relatively wide, 75% of the test section width, in comparison to the wind-tunnel test section. In comparing the static pressure tap located at 2.54 in. from the back surface with the 50,000-Pa value reported by the coupled code solution, here again this value is off by 30,000 Pa. Comparison of the data for the pressure tap located at 1.76 in. from the back surface with the coupled code solution of 50,000 Pa reveals very good agreement. This is because the pressure tap is located more along the centerline of the model and far enough up the wedge front to be unaffected by slight imperfections in the geometry of the nose region or by edge effects. In general except for the edge effects, the coupled code solutions show good agreement with the experimental results obtained for the blunted wedge model. Thus, although the pressure distribution was not accurately predicted by the coupled code (wall affects were not modeled), this had a small impact on heat transfer predictions at the centerline, where temperatures were measured. Finally, Fig. 13 presents the complete static temperature field of both fluid and solid regions for a representative time $t = 5.4$ s. Also in Fig. 13 are the geometry and intial temperatures.

Conclusions

A coupled DRBEM/FVM algorithm was developed for the solution of transient conjugate heat transfer problems. The algorithm avoids meshing of the solid by combining the DRBEM with an FVM flow solver. The boundary-only discretization required by the DRBEM affords a distinct advantage over domain meshing techniques currently proposed for CHT analysis. This is particularly true when the solid geometry is intricate, for example, in cooled turbine blade passage, where maintaining grid othogonality at the wall for accurate wall flux computations is an onerous task. Further, in the DRBEM, the wall heat flux is computed as part of the solution, in contrast to domain meshing methods in which the wall flux is computed in postprocessing by numerical differentiation. Two coupled codes were discussed: The first couples GASP to DRBEM, and the second couples an in-house FVM code to DRBEM. Both FVM codes are implicit and were run using the same Baldwin–Lomax turbulence model and min-mod flux limiter. Verification of the coupled CHT codes was provided under steady-state conditions for flow over a flat plate and in a channel. This paper has also presented details of wind-tunnel experiments that were conducted to gather experimental transient heat transfer data for verification of the transient CHT codes. Wind-tunnel models were fully instrumented to gather both pressure and temperature data. The two coupled DRBEM/FVM conjugate codes were tested, and experimental data were shown to be in agreement with numerical predictions, thus verifying the proposed DRBEM/FVM approach to solving time accurate CHT problems.

Acknowledgments

This work has been partially supported by a research grant from the Florida Space Grant Consortium and Technological Research and Development Authority and Contract N68936-96-C-0240 from the U.S. Naval Air Warfare Center, Weapons Division, China Lake, California.

References

[1]Comini, G., Saro, O., and Manzan, M., "A Physical Approach to Finite-Element Modeling of Coupled Conduction and Convection," *Numerical Heat Transfer*, Pt. B, Vol. 24, No. 2, 1993, pp. 243–261.

[2]Shyy, W., and Burke, J., "Study of Iterative Characteristics of Convective-Diffusive and Conjugate Heat Transfer Problems," *Numerical Heat Transfer*, Pt. B, Vol. 26, No. 1, 1994, pp. 21–37.

[3]Blank, D., "Conjugate Conduction-Convection Heat Transfer Model for the Valve Flow-Field Region of Four-Stroke Piston Engines," *Numerical Heat Transfer*, Pt. A, Vol. 18, No. 3, 1990, pp. 283–308.

[4]Imlay, S. T., Soetrisno, M., and Roberts, D. W., "Coupled Flow and Heat Trasnfer Analysis Using Structured-Unstructured Grids," AIAA Paper 96-0622, 1996.

[5]Kao, K.-H., and Liou, M.-S., "Application of Chimera/Unstructured Hybrid Grids for Conjugate Heat Transfer," *AIAA Journal*, Vol. 35, No. 9, 1997, pp. 1472–1478.

[6]Hassan, B., Kuntz, D., and Potter, D. L., "Coupled Fluid/Thermal Prediction of Ablating Hypersonic Vehicles," AIAA Paper 98-0168, 1998.

[7]Li, H. J., and Kassab, A. J., "Numerical Prediction of Fluid Flow and Heat Transfer Within Turbine Blades with Internal Cooling," AIAA Paper 94-1981, 1994.

[8]Kassab, A. J., and Li, H., "A Combination FVM and BEM Method for Conjugate Heat Transfer Calculations in Turbine Blades," AIAA Paper 94-2933, 1994.

[9]Brebbia, C. A., Telles, J. C. F., and Wrobel, L. C., *Boundary Element Techniques*, Springer–Verlag, Berlin, 1984, Chaps. 1–4.

[10]He, M., Kassab, A. J., Bishop, P. J., and Minardi, A., "A Coupled FDM/BEM Iterative Solution for the Conjugate Heat Transfer Problem in Thick Walled Channels: Constant Temperature Imposed at the Outer Channel Wall," *Engineering Analysis*, Vol. 15, No. 1, 1995, pp. 43–50.

[11]He, M., Bishop, P., Kassab, A. J., and Minardi, A., "A Coupled FDM/BEM Solution for the Conjugate Heat Transfer Problem," *Numerical Heat Transfer, Part B: Fundamentals*, Vol. 28, No. 2, 1995, pp. 139–154.

[12]Kontinos, D., "Coupled Thermal Analysis Method with Application to Metallic Thermal Protection Panels," *Journal of Thermophysics and Heat Transfer*, Vol. 11, No. 2, 1997, pp. 173–181.

[13]Nardini, D., and Brebbia, C. A., "A New Approach to Free Vibration Analysis Using Boundary Elements," *Boundary Element Methods in Engineering*, edited by C. A. Brebbia, Computational Mechanics Publ., Southampton, England, U.K., and Springer–Verlag, Berlin, 1982, pp. 235–247.

[14]Partridge, P. W., Brebbia, C. A., and Wrobel, L. C., *The Dual Reciprocity Boundary Element Method*, Computational Mechanics Publ., Southampton, England, U.K., 1992, Chaps. 2–5.

[15]McGrory, W. D., Slack, D. C., Applebaum, M., and Walters, R. W., GASP, The General Aerodynamic Simulation Program, Ver. 2, AeroSoft, Inc., 1992.

[16]Cavalleri, R. J., and Tiarn, W., "CFD Evaluation of an Advanced Thrust Vector Control Concept," AIAA Paper 90-100, 1990.

[17]Cavalleri, R. J., and Tiarn, W., "PTVC Thermal and Performance Analysis," Applied Technology Associates, Rept. for H. R. Textron, Orlando, FL, Sept. 1991.

[18]Baldwin, B. S., and Lomax, H., "Thin Layer Approximation and Algebraic Model for Separated Turbulent Flow," AIAA Paper 78-257, 1998.

[19]Tannehill, J. C., Anderson, D. A., and Pletcher, R. H., *Computational Fluid Mechanics and Heat Transfer*, 2nd ed., Taylor and Francis, New York, 1997, p. 304.

[20]Whitfield, D. L., "Implicit Upwind Finite Volume Scheme for the Three-Dimensional Euler Equations," Mississippi State Univ., MSSU-EIRS-ASE-85-1, Mississippi State, MS, Sept. 1985.

[21]Whitfield, D. L., and Janus, J. M., "Three-Dimensional Unsteady Euler Equation Solutions Using Flux Vector Splitting," AIAA Paper 84-1552, 1984.

[22]Rizzo, F., and Shippy, D. J., "A Method of Solution for Certain Problems of Transient Heat Conduction," *AIAA Journal*, Vol. 8, No. 11, 1970, pp. 2004–2009.

[23]Powell, M. J. D., "The Theory of Radial Basis Function Approximation," *Advances in Numerical Analysis*, edited by W. Light, Vol. 2, Oxford Science, Oxford, 1992, pp. 143–167.

[24]Bialecki, R., and Nowak, A. J., "Boundary Value Problems for Non-linear Material and Non-linear Boundary Conditions," *Applied Mathematical Modeling*, Vol. 5, No. 4, 1981, pp. 417–421.

[25]Brebbia, C. A., and Nowak, A. J., "Solving Heat Transfer Problems by the Dual Reciprocity BEM," *Boundary Elements in Heat Transfer*, edited by L. C. Wrobel and C. A. Brebbia, Computational Mechanics Publ., Southampton, England, U.K., and Elsevier Applied Science, New York, 1992, Chap. 1.

[26]Rahaim, C. P., "A Coupled Finite volume/DRBEM Solution for Transient Non-linear Conjugate Heat Transfer Problems in Compressible Flows," Ph.D. Dissertation, Mechanical and Aerospace Engineering Dept., Univ. of Central Florida, Orlando, FL, July 1996.

[27]Rahaim, C. P., and Kassab, A. J., "Application of the DRBEM to the Solution of Viscous Fluid Flow in a Channel," *Proceedings of BETECH94, the 9th International Conference on Boundary Element Technology*, edited by C. A. Brebbia and A. J. Kassab, Computational Mechanics Publ., Southampton, England, U.K., 1994, pp. 147–154.

[28]Rahaim, C. P., and Kassab, A. J., "A DRBEM Solution for Incompressible Viscous Flows and Heat Transfer," AIAA Paper 95-2113, 1995.

[29]Rahaim, C. P., and Kassab, A. J., "Pressure Correction DRBEM Solution for Heat Transfer and Fluid Flow in Incompressible Viscous Flows," *Engineering Analysis with Boundary Elements*, Vol. 18, No. 4, 1996, pp. 265–272.

[30]Schetz, J. A., *Boundary Layer Analysis*, Prentice–Hall, Upper Saddle River, NJ, 1993, Chaps. 5 and 10.

[31]Pozzi, A., and Lupo, M., "The Coupling of Conduction with Forced Convection in Graetz Problems," *Journal of Heat Transfer*, Vol. 12, July 1990, pp. 323–328.